This manuscript was prepared for Atmos. Chem. Phys. (Discuss.)
with the egs LaTeX class egs.cls version 6.1 from 2001/09/03.

ACP-LOGO

Imaging Gravity Waves in Lower Stratospheric AMSU-A Radiances

S. D. Eckermann[1], D. Wu[2], J. D. Doyle[3], L. Coy[1], J. P. McCormack[1], A. Stephens[4], B. N. Lawrence[4], and T. F. Hogan[5]

[1]E.O. Hulburt Center for Space Research, Naval Research Laboratory, Washington, DC, USA
[2]Jet Propulsion Laboratory, California Institute of Technology, Pasadena, California, USA
[3]Marine Meteorology Division, Code 7531, Naval Research Laboratory, Monterey, CA, USA
[4]British Atmospheric Data Center, Rutherford Appleton Laboratory, Oxfordshire, UK
[5]Marine Meteorology Division, Code 7532, Naval Research Laboratory, Monterey, CA, USA

ACPD: Received: ??? – Published: ???
ACP: Received: ??? – Accepted: ??? – Published: ???

Abstract.
TO APPEAR IN SPARC NEWSLETTER

1 Introduction

Gravity waves drive important aspects of the global stratospheric circulation, climate and chemical state (e.g., Fritts and Alexander, 2003; Alexander and Rosenlof, 2003; Mann et al., 2005), and thus are a focus area for SPARC. The satellite remote sensors and global models so crucial to increased understanding of larger-scale stratospheric dynamics have (until recently) lacked the necessary horizontal and vertical resolutions to resolve gravity waves and gravity wave breaking. As a result, the observational record on stratospheric gravity waves has relied mostly on suborbital observations at scattered locations around the globe. This has motivated several SPARC activities: e.g., an initiative to record radiosonde data at higher resolution to resolve gravity wave motions better (Vincent, 2003; Wang and Geller, 2003), and field programs to observe and understand gravity wave generation from deep convection (Hamilton et al., 2004). The inability of global models to fully resolve gravity wave dynamics has also led to SPARC-sponsored workshops aimed at improving subgridscale gravity wave parameterizations for these models (Hamilton, 2004), and GRIPS studies of the energy spectra of resolved dynamics in global models (Koshyk et al., 1999).

Advances in both computing power and remote-sensing technology are now yielding higher resolution global model fields and satellite data from the stratosphere that can explicitly resolve some of the long wavelength "outer scales" of the gravity wave spectrum (e.g., Hamilton et al., 1999; Wu et al., 2005). Here we provide a preliminary report on the gravity wave detection and imaging capabilities of the Advanced Microwave Sounding Unit's (AMSU-A) lower stratospheric temperature channels.

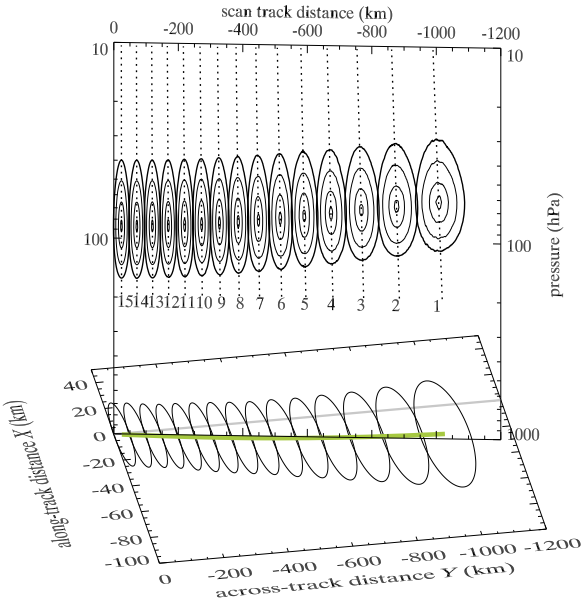

Fig. 1. Two-dimensional cross sections of modeled Channel 9 weighting functions, plotted versus pressure, cross-track distance Y and along-track distance X for beam positions $j = 1 \ldots 15$. Thick contours show half-power levels, which are projected to the surface to depict horizontal footprints. Other contours show the 70%, 90% and 99% levels. Dotted lines show line-of-sight ray paths from the peaks in each weighting function to the satellite.

Correspondence to: S. D. Eckermann (stephen.eckermann@nrl.navy.mil)

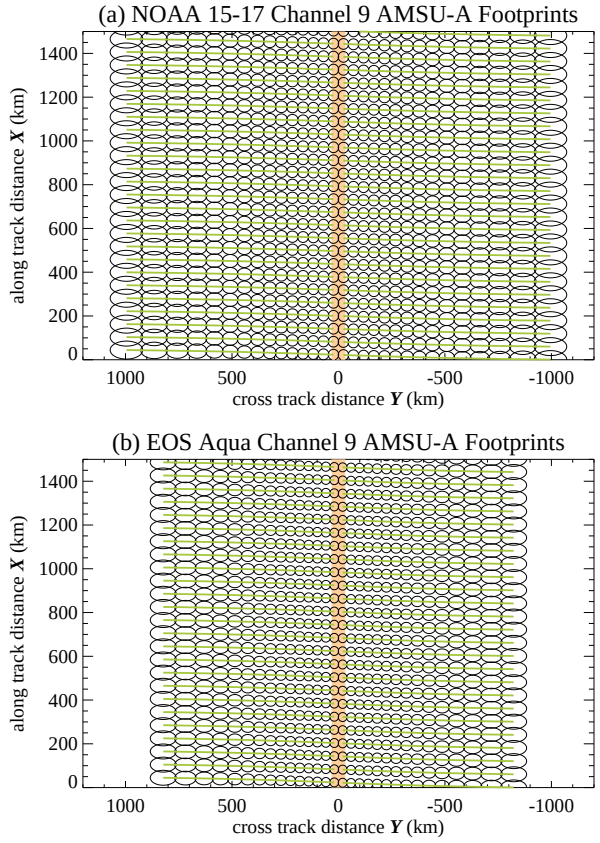

Fig. 2. AMSU-A Channel 9 horizontal footprints traced out as a function of along-track and cross-track distances by the AMSU-A scanning measurements from (a) NOAA-15 through NOAA-17 satellites and (b) EOS Aqua. Orange line shows the satellite ground track. Green curves show the scanning pattern from right-to-left across Y as the satellite moves at along X, with footprints at each beam position j overlayed.

2 Background and Motivation

The stratosphere contains a spectrum of many gravity waves which span a wide range of propagation directions and wavelengths. Those few remote-sensing instruments that have resolved gravity waves to date do so only at the very longest wavelength portions of this spectrum, and thus measure only a small fraction of the total wave variance. Furthermore, each instrument's "visibility" to waves is generally a complex three-dimensional function of channel, orbit position, viewing direction and atmospheric location. To complicate matters further, the wavelengths of individual gravity waves also vary significantly via refraction by the background flow. Thus, different waves are constantly moving into and out of the narrow visibility windows of the instrument. Such effects have made these new gravity wave signals challenging to analyze and to compare with model predictions (Alexander, 1998; Jiang et al., 2004; Wu et al., 2005).

Furthermore, satellite gravity wave data acquired to date often resemble a global distribution of suborbital measurements, in the sense that they provide only a one-dimensional cross section through three-dimensional wave fields. For example, some limb instruments yield vertical temperature profiles with wave oscillations superimposed that resemble a sequence of radiosonde profiles (Eckermann and Preusse, 1999; Tsuda et al., 2000). Others yield high-resolution measurements at a given altitude along the orbital track that contain wave fluctuations, similar to aircraft data (Wu and Waters, 1996; Jiang et al., 2004).

We need new generations of satellite instruments that can improve upon these initial observations. Specifically, we seek data with well-defined visibility characteristics that permit meaningful physical interpretation of the wave signals, and that provide two-dimensional or even three-dimensional views of the wave fields.

3 Advanced Microwave Sounding Unit-A

The Advanced Microwave Sounding Unit (AMSU) is a passive microwave scanner currently deployed on five different satellites: the NOAA 15 through 18 meteorological satellites (Kidder et al., 2000), and NASA's Earth Observation System (EOS) Aqua satellite (Lambrigtsen, 2003). The instrument scans across the satellite track in 30 sequential step-and-stare measurements at equispaced off-nadir scan angles between $\pm 48.33^{\circ}$. The AMSU-A module has 15 measurement channels, 6 of which (Channels 9–14) are stratospheric temperature channels measuring O_2 wing line emissions centered at 57.29 GHz.

To model how gravity waves might appear in AMSU-A radiances, we've developed a simplified model of the AMSU-A radiance acquisition that yields three-dimensional temperature weighting functions, which we've validated against more detailed modeling results: see Wu (2004) and Eckermann and Wu (2005) for complete details. Figure 1 shows cross-sections of the derived Channel 9 weighting functions at 15 adjacent scan angles for the AMSU-A on the NOAA satellites. They show radiances from the near-nadir beams peaking at $\sim$80-90 hPa, while those at the largest scan angles peak higher at $\sim$60-70 hPa due to the limb effect (Goldberg et al., 2001). Figure 1 also shows the horizontal measurement footprints, specified by 50% contours of the weighting functions at the altitude of peak response. Figure 2a shows how the scanning pattern and the 7.4 km s^{-1} velocity of the NOAA satellites maps these footprints into a pixelated two-dimensional radiance map with a cross-track width of $\sim$2100 km. The lower orbit altitude of EOS Aqua yields smaller footprints and cross-track swath widths (Figure 2b).

4 Simple Forward Modeling

Each AMSU-A measurement yields a brightness temperature

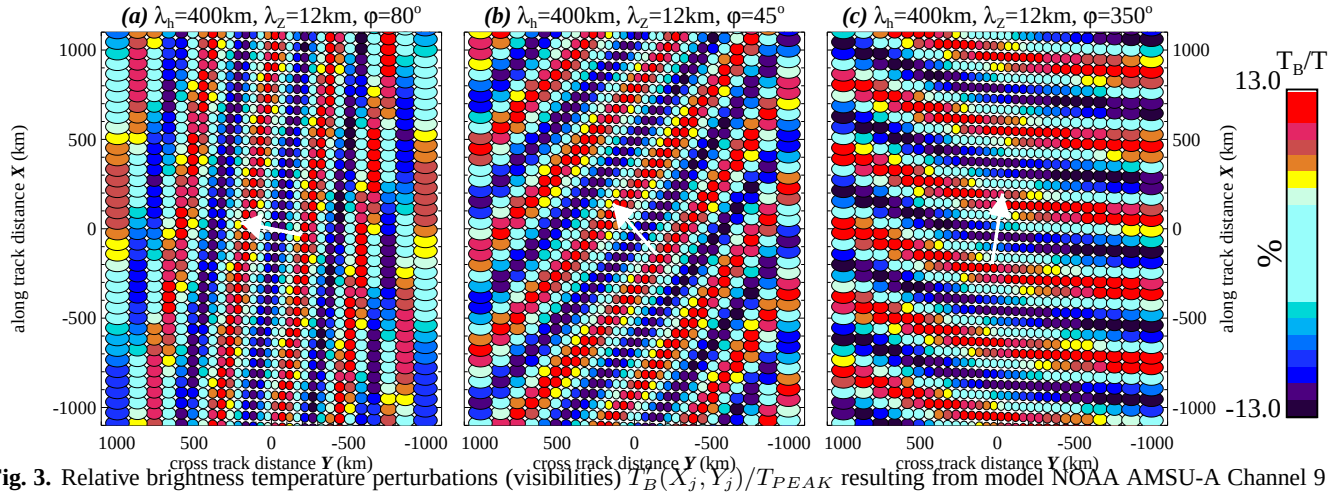

Fig. 3. Relative brightness temperature perturbations (visibilities) $T'_B(X_j, Y_j)/T_{PEAK}$ resulting from model NOAA AMSU-A Channel 9 sampling of (2) with $\lambda_h = 400$ km, $\lambda_Z = 12$ km, and φ values of (a) 80°, (b) 45°, and (c) 350°. The white vector at the center of each plot shows the direction of horizontal wave propagation φ. The color scale is visibility expressed as a percentage.

$$T_B(X_j, Y_j) = \int_{-\infty}^{\infty} \int_{-\infty}^{\infty} \int_{0}^{Z_{sat}} W_j(X - X_j, Y - Y_j, Z) \, T(X, Y, Z) dX dY dZ, \quad (1)$$

that characterizes the radiance via the Rayleigh-Jeans approximation to the Planck function. $T(X, Y, Z)$ is the atmospheric temperature field, Z is pressure height, X and Y are along-track and cross-track distances. To assess the instrument's ability to detect gravity waves, we specified infinite three-dimensional monochromatic gravity wave temperature oscillations

$$T'(X, Y, Z) = T_{PEAK} \cos\left(k_X X + k_Y Y + k_Z Z\right), \quad (2)$$

where T_{PEAK} is the peak temperature amplitude. We varied the vertical wavelength $\lambda_Z = 2\pi/|k_Z|$, horizontal wavelength $\lambda_h = 2\pi/k_h$, and horizontal propagation angle φ with respect to the AMSU-A scan axes (X, Y, Z), where $k_X = \pm 2\pi/\lambda_X = k_h \cos\varphi$, $k_Y = \pm 2\pi/\lambda_Y = k_h \sin\varphi$, and $k_Z < 0$. We then used (2) as the temperature field in (1) and evaluated this integral numerically at each measurement location (X_j, Y_j) using realistic scanning patterns.

Figure 3 plots resulting NOAA AMSU-A perturbation brightness temperatures $T'_B(X_j, Y_j)$ for a wave of $\lambda_h = 400$ km and $\lambda_Z = 12$ km, propagating in three different directions. The results are plotted as a normalized "visibility" $T'_B(X_j, Y_j)/T_{PEAK}$, and show peak values of ∼13%. Thus, a gravity wave of this type with a peak temperature amplitude T_{PEAK}=5 K would yield oscillations in Channel 9 brightness temperatures of ∼0.65 K in amplitude, according to the model. Since nominal Channel 9 noise floors are ∼0.16 K (Lambrigtsen, 2003; Wu, 2004), this wave signal is (theoretically) large enough to appear in the measurements.

Though the response is not always uniform across the swath and some distortion of wave phase lines is produced by limb effects (Eckermann and Wu, 2005), Figure 3 predicts that this wave is imaged horizontally by the radiance maps swept out by the AMSU-A scanning pattern.

5 AMSU-A Measurements on 14 January 2003

Figure 4 plots perturbations in Channel 9 brightness temperatures, $T'_B(\hat{\lambda}_j, \hat{\phi}_j)$, acquired by AMSU-A during overpasses of Scandinavia by Aqua, NOAA-15, NOAA-16 and NOAA-17 on 14 January 2003. Here $(\hat{\lambda}_j, \hat{\phi}_j)$ are the longitudes and latitudes of the various measurement footprints. The perturbations were extracted from raw radiances by computing and then subtracting a large-scale radiance field (see Eckermann et al., 2005, for details).

At ∼0116 UTC and 0226 UTC, the perturbation maps are essentially featureless, with values near nominal noise floors. During the 0650 UTC NOAA-15 overpass, Figure 4c shows the first suggestions of a wavelike oscillation over southern Scandinavia (note the change in color scale from ±0.3 K to ±0.6 K in the maps at this time). In subsequent AMSU-A overpasses at 1033 UTC, 1221 UTC and 1229 UTC, this oscillation grows in amplitude to a maximum of ∼0.9 K. In the final two measurements at 1641 UTC and 2023 UTC the amplitude weakens slightly, but also changes it's horizontal structure, acquiring a longer wavelength that is aligned differently and has a packet width that is noticeably more extended in the along-phase direction

6 NWP Model Simulations

A three-dimensional description of the wave temperature field is needed to model the AMSU-A radiance signal. Thus we analyzed output from high-resolution numerical weather prediction (NWP) models that might resolve any wave-

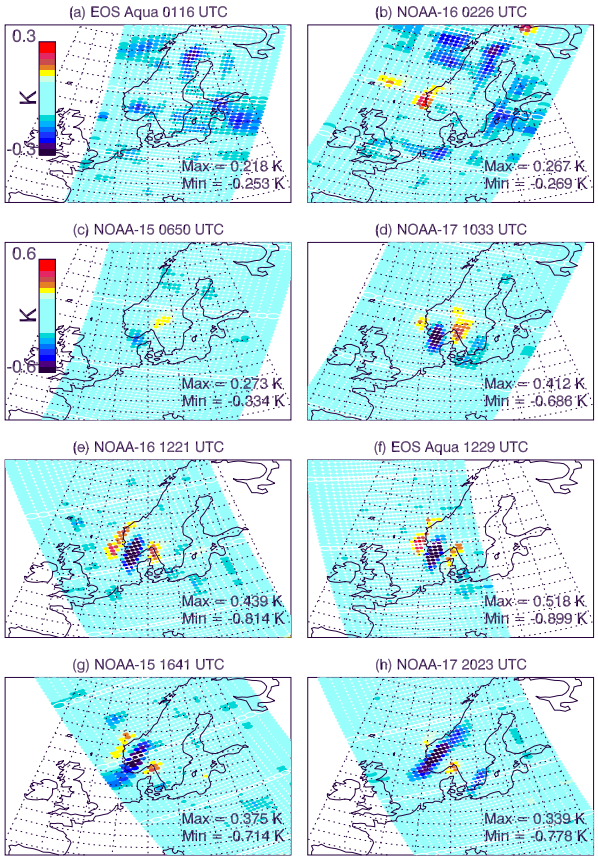

Fig. 4. AMSU-A Channel 9 brightness temperature perturbations $T'_B(\hat{\lambda}_j, \hat{\phi}_j)$ in Kelvin: for panels (a) and (b), the range is ± 0.3 K, for panels (c)–(h) the color bar range is ± 0.6 K. The panels are arranged in chronological order: the universal time and platform of each overpass is given in each plot title. Data are plotted as color-coded footprint ellipses at the measurement location. White curves outline these measurement footprints for every tenth scan. Maximum and minimum values for each map are shown in the lower-right portion of each panel. We applied 3x3 point smoothing to suppress gridpoint noise.

induced temperature perturbations in the stratosphere over Scandinavia at this time. We used:

(a) archived 6 hourly operational forecast fields from the European Centre for Medium-Range Weather Forecasts (ECMWF) Integrated Forecast System's (IFS) $T_L511L60$ global spectral model (Untch and Hortal, 2004).

(b) hourly hindcast fields from a developmental T239L60 version of the Navy Operational Global Atmospheric Prediction System (NOGAPS) global spectral forecast model with Advanced Level Physics and High Altitude (NOGAPS-ALPHA: Eckermann et al., 2004).

(c) hourly hindcast fields from a nested 10x10 km^2 hindcast run using the Naval Research Laboratory Coupled Ocean/Atmosphere Mesoscale Prediction System (COAMPS^{TM}: Hodur, 1997).

All the model runs were initialized on 13 January 2003 at 1200 UTC. Further details are given in Eckermann et al. (2005). Each model run brought something unique to this study. For example, the high spatial resolution of the COAMPS fields was expected to be sufficient to model any waves AMSU-A might resolve, whereas the lower resolution NOGAPS-ALPHA and ECMWF IFS global fields were expected to resolve waves but underestimate their amplitudes (Skamarock, 2004). Yet unlike the global models, COAMPS could not produce output over the full geographical range of AMSU-A data plotted in Figure 4, nor to middle and upper stratospheric altitudes.

The upper two rows of Figure 5 plot temperature perturbations $T'(\hat{\lambda}, \hat{\phi}, p)$ at $p = 90$ hPa extracted from the three NWP models' +24 hour forecast fields, valid at 1200 UTC on 14 January. They show a mountain wave oscillation over southern Scandinavia with a geographical extent and phase structure that resembles the 1200 UTC AMSU-A data in Figures 4e and 4f.

The bottom panels of Figure 5 plot altitude cross-sections of the temperature fields along the horizontal black line plotted in the panels above. Each model produces a similar-looking mountain wave oscillation that grows in amplitude up to 10 hPa and beyond. The horizontal wavelength λ_h is $\sim$400 km and vertical wavelength λ_Z is $\sim$12 km.

7 Conversion to Brightness Temperatures

We convert the NWP temperature fields into synthetic Channel 9 brightness temperatures $T_{B_{NWP}}(\hat{\lambda}_j, \hat{\phi}_j)$ by numerically evaluating (1) on the sphere using the actual AMSU-A scan patterns over Scandinavia, using methods outlined by Eckermann et al. (2005). We then isolate brightness temperature perturbations $T'_{B_{NWP}}(\hat{\lambda}_j, \hat{\phi}_j)$ using exactly the same data reduction algorithms that we applied to the radiance data to produce Figure 4.

Figure 6 plots resulting $T_{B_{NWP}}(\hat{\lambda}_j, \hat{\phi}_j)$ fields using 1200 UTC NWP fields profiled in Figure 5, based on the 1221 UTC NOAA-16 and 1229 UTC EOS Aqua overpass scans, whose data are reproduced in the far right panels. All 3 NWP models reproduce a wave oscillation over southern Scandinavia with similar amplitude, phase and packet structures to those measured by AMSU-A. Figure 7 plots $T_{B_{NWP}}(\hat{\lambda}_j, \hat{\phi}_j)$ maps based on the closest hourly NOGAPS-ALPHA fields to each corresponding measurement in Figure 4. The structure in each panel of Figure 7 resembles that seen in the AMSU-A data in Figure 4, especially the evolution of the resolved wave pattern from 0700 UTC to 2000 UTC, though amplitudes in Figure 7 are somewhat weaker. Corresponding maps using COAMPS temperatures (not shown) yield larger amplitudes that are closer to the observations.

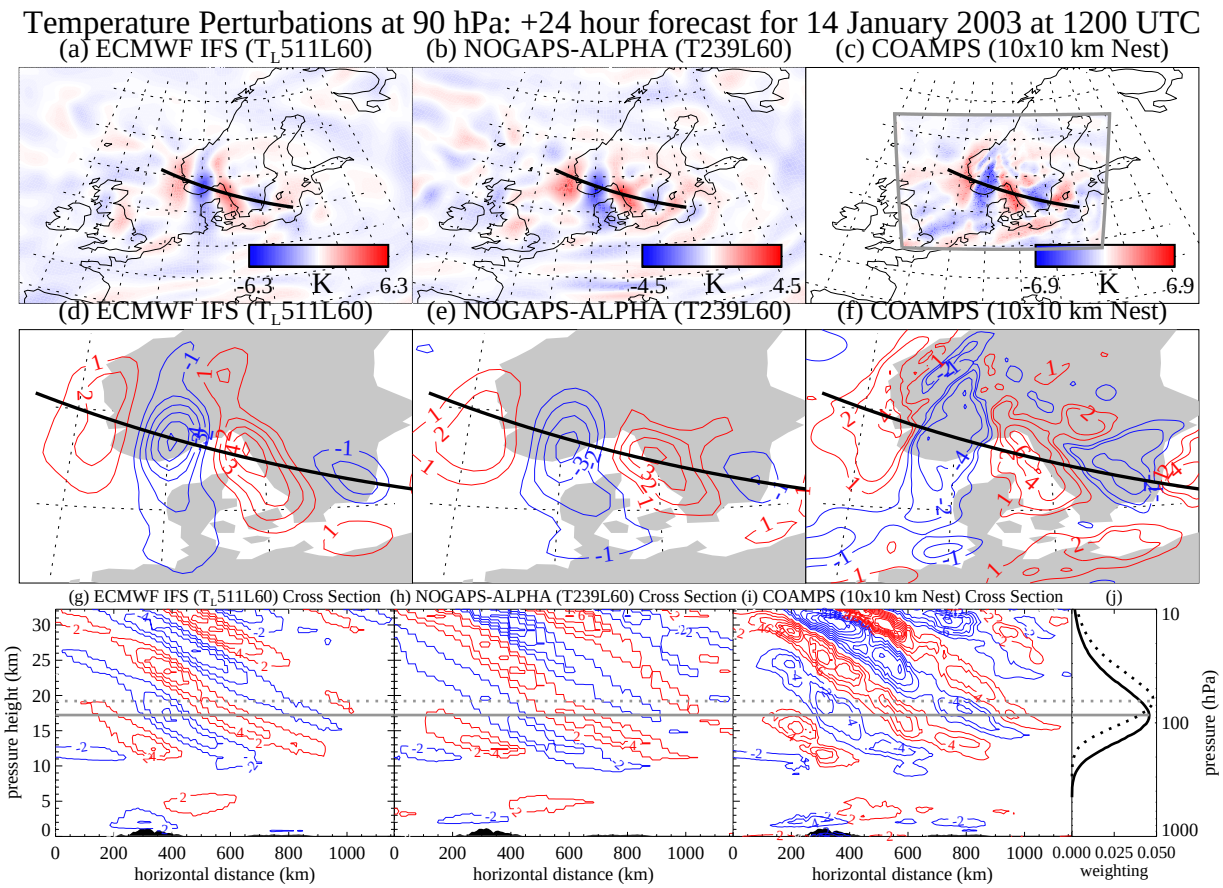

Fig. 5. Top row plots temperature perturbations $T'(\hat{\lambda}, \hat{\phi}, p)$ at $p = 90$ hPa extracted from +24 hour forecasts from ECMWF IFS (left column), NOGAPS-ALPHA (middle column) and COAMPS (right column) runs. See color bar in the lower-right corner of each panel for temperature range. Middle row plots same fields, but now focused over southern Scandinavia. Contour interval is 1 K. Bottom row of plots show altitude contours of $T'(\lambda, \phi, p)$ along the horizontal cross section plotted as black curve in the panels above. Negative (cold) temperature anomalies are blue, positive (warm) temperature anomalies are red, and the contour interval is 2 K (zero contour is omitted). Cross-sections of topographic surface elevations are shaded in gray. Panel j shows AMSU-A Channel 9 1D vertical weighting functions at the near-nadir position (solid) and far off-nadir position (dotted).

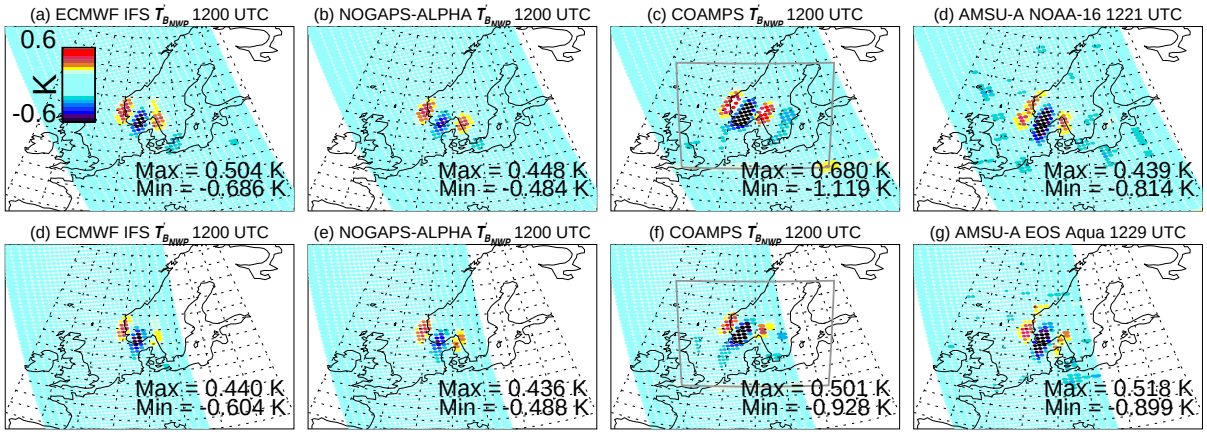

Fig. 6. Top row: brightness temperature perturbations $T'_{BNWP}(\hat{\lambda}_j, \hat{\phi}_j)$ extracted from 1200 UTC (+24 hour) NWP temperature fields $T(\hat{\lambda}, \hat{\phi}, p)$ from (a) ECMWF IFS, (b) NOGAPS-ALPHA, and (c) COAMPS runs, using the AMSU-A scan pattern from the NOAA-16 1221 UTC overpass. The data from Figure 4e are replotted in panel d. Bottom row shows same sequence of plots for the 1229 UTC EOS Aqua overpass. Gray squares in (c) and (f) show the regional COAMPS domain. Color bar scale ($\pm$0.6 K) is given at the top-left of panel a. Maximum and minimum values for each map are shown in the lower-right portion of each panel.

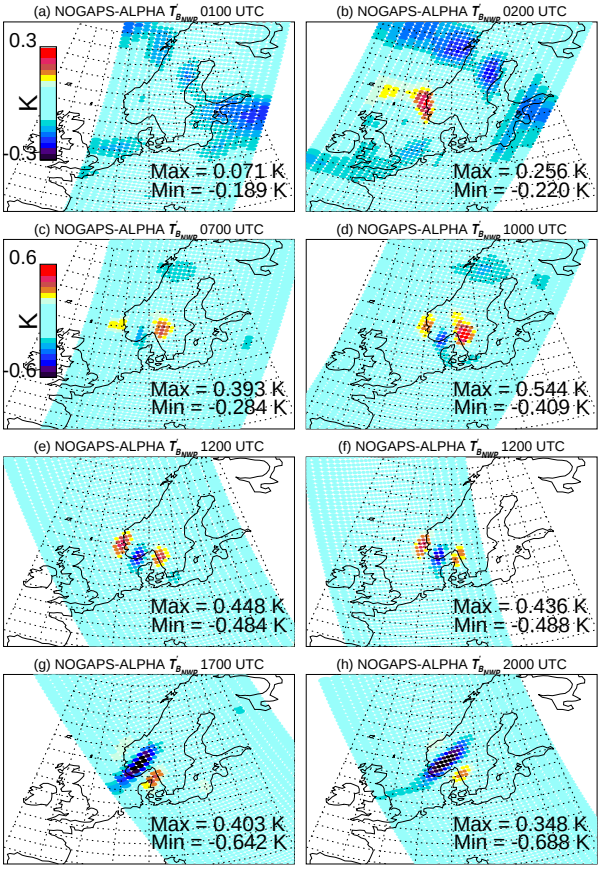

Fig. 7. Similar presentation to Figure 4, but showing brightness temperature perturbations $T'_{B_{NWP}}(\hat{\lambda}_j, \hat{\phi}_j)$ derived from hourly NOGAPS-ALPHA temperature fields closest to the satellite overpass in question. Values are in Kelvin (see color bars): for panels (a) and (b) the range is ± 0.3 K, whereas for panels (c)–(h) the color bar range is ± 0.6 K. Maximum and minimum values for each map are shown in the lower-right portion of each panel.

8 Summary and Outlook

These comparisons prove that the radiance perturbations extracted from the AMSU-A Channel 9 measurements in Figure 4 are stratospheric gravity waves, and they validate our model predictions of the anticipated radiance signals based on our derived weighting functions. This work supports preliminary experimental studies by Wu (2004) and Wu and Zhang (2004) who found apparent gravity wave oscillations in radiances from AMSU-A's stratospheric channels.

The comparisons also show that the global ECMWF IFS and NOGAPS-ALPHA NWP models explicitly resolved the gravity wave observed over Scandinavia on 14 January 2003, though they underpredicted its amplitude. Based on each global model's horizontal resolution, this $\lambda_h \sim$400 km wave is expected to suffer some amplitude attenuation from the effects of scale-dependent numerical dissipation operating on the smallest resolved scales (Skamarock, 2004). Further comparisons like these among gravity wave fields explicitly resolved by models and satellite instruments should help to improve our understanding and description of stratospheric gravity wave dynamics.

The modeling results also suggest that other current and future cross-track scanners have resolutions comparable to or better than AMSU-A that should allow them to resolve and image stratospheric gravity waves too. Examples on the microwave side are the Special Sensor Microwave Imager/Sounder (SSMIS) on the Defense Meteorological Satellite Program (DMSP) satellite, and the Advanced Technology Microwave Sounder (ATMS) and Conical Scanning Microwave Imager/Sounder (CMIS) slated to fly on the National Polar-orbiting Operational Environmental Satellite System (NPOESS). Another interesting example is the Advanced Infrared Sounder (AIRS), which operates in comanifested form with AMSU-A on EOS Aqua with a scan pattern of 90 sequential step and stare measurements with horizontal footprint diameters three times smaller than AMSU-A. These properties should allow AIRS to image smaller horizontal wavelength gravity waves than AMSU-A.

Acknowledgements. none yet...

References

Alexander, M. J.: Interpretations of observed climatological patterns in stratospheric gravity wave variance, J. Geophys. Res., 103, 8627-8640, 1998.

Alexander, M. J., and Rosenlof, K. H.: Gravity-wave forcing in the stratosphere: Observational constraints from the Upper Atmosphere Research Satellite and implications for parameterization in global models, J. Geophys. Res., 108(D19), 4597, doi:10.1029/2003JD003373, 2003.

Eckermann, S. D., and Preusse, P.: Global measurements of stratospheric mountain waves from space, Science, 286, 1534–1537, 1999.

Eckermann, S. D., and Wu, D.: Imaging gravity waves in lower stratospheric AMSU-A radiances, Part 1, Simple forward model, (paper in preparation), 2005.

Eckermann, S. D., McCormack, J. P., Coy, L., Allen, D., Hogan, T., and Kim, Y.-J.: NOGAPS-ALPHA: A prototype high-altitude global NWP model, *Preprint Vol. Symposium on the 50th. Anniversary of Operational Numerical Weather Prediction*, American Meteorological Society, University of Maryland, College Park, MD, 14-17 June, Paper P2.6, 23pp, 2004. [Available online at http://uap-www.nrl.navy.mil/dynamics/papers/Eckermann_P2.6-reprint.pdf.]

Eckermann, S. D., Wu, D., Doyle, J. D., Coy, L., Lawrence, B. N., Stephens, A., McCormack, J. P., and Hogan, T. F.: Imaging gravity waves in lower stratospheric AMSU-A radiances, Part 2, Validation case study, (paper in preparation), 2005.

Fritts, D. C., and Alexander, M. J., Gravity wave dynamics and effects in the middle atmosphere, Rev. Geophys., 41(1), 1003, doi:10.1029/2001RG000106, 2003.

Goldberg, M. D., Crosby, D. S., and Zhou, L.: The limb adjustment of AMSU-A observations: methodology and validation, J. Appl. Meteor., 40, 70–83, 2001.

Hamilton, K.: Report on Chapman Conference on Gravity Wave Processes and Parameterization, SPARC Newsletter, 23, 15–19, 2004.

Hamilton, K., Wilson, R. J., and Hemler, R. S.: Middle atmosphere simulated with high vertical and horizontal resolution versions of a GCM: improvements in the cold pole bias and generation of a QBO-like oscillation in the tropics, J. Atmos. Sci., 56, 3829–3846, 1999.

Hamilton, K., Vincent, R. A., and May, P. T.: Darwin Area Wave Experiment (DAWEX) field campaign to study gravity wave generation and propagation, J. Geophys. Res., 109, D20S01, doi:10.1029/2003JD004393, 2004.

Hodur, R. M.: The Naval Research Laboratory's Coupled Ocean/Atmosphere Mesoscale Prediction System (COAMPS), Mon. Wea. Rev., 125, 1414–1430, 1997.

Jiang, J. H., Eckermann, S. D., Wu, D. L., and Ma, J.: A search for mountain waves in MLS stratospheric limb radiances from the Northern Hemisphere: data analysis and global mountain wave modeling, J. Geophys. Res., 109, D03107, doi:10.1029/2003JD003974, 2004.

Kidder, S. Q., Goldberg, M. D., Zehr, R. M., DeMaria, M., Purdom, J. F. W., Velden, C. S., Grody, N. C., and Kusselson, S. J.: Satellite analysis of tropical cyclones using the Advanced Microwave Sounding Unit (AMSU), Bull. Amer. Meteorol. Soc., 81, 1241–1259, 2000.

Koshyk, J. N., Boville, B. A., Hamilton, K., Manzini, E., and Shibata, K.: Kinetic energy spectrum of horizontal motions in middle-atmosphere models, J. Geophys. Res., 104, 27,177–27,190, 1999.

Lambrigtsen, B. H.: Calibration of the AIRS microwave instruments, IEEE Trans. Geosci. Remote Sens., 41, 369–378, 2003.

Mann, G. W., Carslaw, K. S., Chipperfield, M. P., Davies, S., and Eckermann, S. D., Large NAT particles and denitrification caused by mountain waves in the Arctic stratosphere, J. Geophys. Res., 110, D08202, doi:10.1029/2004JD005271, 2005.

Skamarock, W. C.: Evaluating mesoscale NWP models using kinetic energy spectra. Mon. Wea. Rev., 132, 3019–3032, 2004.

Tsuda, T., Nishida, M., Rocken, C., and Ware, R. H.: A global morphology of gravity wave activity in the stratosphere revealed by the GPS occultation data (GPS/MET), J. Geophys. Res., 105, 7257–7273, 2000.

Untch, A., and Hortal, M.: A finite-element scheme for the vertical discretization of the semi-Lagrangian version of the ECMWF forecast model, Quart. J. Roy. Meteor. Soc., 130, 1505–1530, 2004.

Vincent, R. A.: Status of the SPARC radiosonde initiative, SPARC Newsletter, 20, 2003. [available online at http://www.atmosp.physics.utoronto.ca/SPARC/News20/20_Vincent.html]

Wang, L., and Geller, M. A.: Morphology of gravity-wave energy as observed from 4 years (1998-2001) of high vertical resolution U. S. radiosonde data, J. Geophys. Res., 108(D16), 4489, doi:10.1029/2002JD002786, 2003.

Wu, D. L.: Mesoscale gravity wave variances from AMSU-A radiances, Geophys. Res. Lett., 31, L112114, doi:10.1029/2004GL019562, 2004.

Wu, D. L., and Waters, J. W.: Gravity-wave-scale temperature fluctuations seen by the UARS MLS, Geophys. Res. Lett., 23, 3289–3292, 1996.

Wu, D. F., and F. Zhang, A study of mesoscale gravity waves over the North Atlantic with satellite observations and a mesoscale model, J. Geophys. Res., 109, D22104, doi:10.1029/2004JD005090, 2004.

Wu, D. L., Preusse, P., Eckermann, S. D., Jiang, J. H., de la Torre Juarez, M., Coy, L., and Wang, D. Y.: Remote sounding of atmospheric gravity waves with satellite limb and nadir techniques, *Adv. Space Res.*, (in press), 2005.